INSTITUTE OF PHYSICS PUBLISHING SMART MATERIALS AND STRUCTURES
Smart Mater. Struct. **10** (2001) 240–251 www.iop.org/Journals/sm PII: S0964-1726(01)20964-1

Exact solution for the cylindrical bending of laminated plates with embedded piezoelectric shear actuators

Senthil S Vel[1] **and R C Batra**[2]

[1] Department of Mechanical Engineering, University of Maine, Orono, ME 04401-5711, USA
[2] Department of Engineering Science and Mechanics,
Virginia Polytechnic Institute and State University, Blacksburg, VA 24061-0219, USA

Received 7 March 2000, in final form 8 November 2000

Abstract
An exact three-dimensional state space solution is obtained for the static cylindrical bending of simply supported laminated plates with embedded shear mode piezoelectric actuators, and subjected to mechanical and electric loading on the upper and lower surfaces. Each layer of the laminate is made of either an orthotropic elastic material or a piezoelectric material whose poling direction lies in the plane of the plate, with perfect bonding between the adjoining layers. The displacements and stresses for a homogeneous piezoelectric plate for various length-to-thickness ratios are compared with those obtained by the first-order shear deformation theory. Results are also presented for a hybrid laminate with a shear mode piezoelectric core sandwiched between two elastic layers. A comparison of stresses with those in the corresponding surface-mounted extension actuation configuration shows that the longitudinal and shear stresses within the actuator are significantly smaller for the shear actuation mechanism. The analytical results can be used to assess the accuracy of different plate theories and/or validating finite element codes.

1. Introduction

In recent years, piezoelectric materials have been integrated with structural systems to form a class of 'smart structures'. The piezoelectric materials are capable of altering the structure's response through sensing, actuation and control. By integrating surface-bonded and embedded actuators into structural systems, desired localized strains may be induced by applying the appropriate voltage to the actuators.

Piezoelectric actuators in an adaptive structure are usually bonded to the surfaces of the host structure. The application of an electric field causes the actuators to elongate or contract thus forcing the host structure to deform. Such surface-bonded actuators that induce longitudinal strains are known as *extension actuators*. In order to successfully incorporate extension actuators into a structure, the mechanical interaction between the actuators and the host structure must be fully understood. Mechanical models were developed by Crawley and de Luis [1], Crawley and Anderson [2] and others for piezoelectric patches bonded to a beam. Lee [3], Huang and Wu [4], Mitchell and Reddy [5] and others have developed plate theories for rectangular hybrid laminates. Numerous finite element analyses have also been conducted (e.g. see Heyliger *et al* [6], Robbins and Reddy [7], and Batra and Liang [8]). Ray *et al* [9] and Heyliger and Brooks [10] have obtained exact three-dimensional solutions for the cylindrical bending of simply supported piezoelectric laminates. Exact solutions for simply supported rectangular laminates were given by Heyliger [11, 12], Bisegna and Maceri [13], and Lee and Jiang [14]. Yang *et al* [15] and Batra *et al* [16, 17] have used a similar technique to analyse the vibrations of a simply supported plate with piezoceramic actuators either bonded to its upper and lower surfaces or embedded within the laminate. Recently, Vel and Batra [18, 19] have derived three-dimensional analytical solutions for thick piezoelectric plates subjected to various mechanical and electrical boundary conditions at the edges.

All the aforementioned studies deal with piezoelectric extension actuators that are poled in the thickness direction and usually placed at the extreme thickness positions of a plate-like structure to achieve effective actuation. This subjects the actuators to high longitudinal stresses that may be detrimental to the brittle piezoceramic material. Furthermore, surface-bonded actuators are likely to be damaged by contact with surrounding objects. To alleviate these problems Sun and

Zhang [20] proposed an adaptive sandwich structure consisting of an axially poled piezoelectric core sandwiched between two elastic sheets. The application of an electric field in the thickness direction would induce transverse shear deformation of the core, thus generating the desired transverse deflection of the sandwich structure. Piezoelectric actuators poled in such a way as to produce transverse shear deformation are called *shear actuators*. Zhang and Sun [21, 22] developed a beam theory for shear actuated laminates by modelling the facing sheets as classical Euler–Bernoulli beams and the central core as a Timoshenko beam which allows transverse shear deformation. They state that it is very difficult to find a general solution for fully coupled electromechanical equations of a sandwich beam. Benjeddou *et al* [23] developed a unified finite element model for extension and shear actuation mechanisms with more detailed formulation of the electric problem. Aldraihem and Khdeir [24] have used the first-order beam theory and a higher-order beam theory to model smart beams with piezoelectric shear actuators. Benjeddou *et al* [25] have presented the formulation and validation of a new adaptive sandwich-beam finite element. Theoretical and finite element models for the vibration control of sandwich beams with shear actuators are presented by Trindade *et al* [26]. Their results suggest that shear actuators can be more effective than extension actuators for the control of bending vibrations. Benjeddou *et al* [27] compare the extension and shear actuation mechanism for cantilever beams with segmented actuators with the help of an adaptive sandwich beam finite element. Vidoli and Batra [28] have developed a plate theory for an anisotropic piezoelectric plate that accounts for changes in the thickness of the plate caused by the double forces without moments applied to the top and bottom surfaces of the plate. They used this theory for studying numerically the cylindrical bending of a transversely isotropic plate with the axis of transverse isotropy making an angle α with the normal to the midsurface of the plate, and presented results for different values of α. For $\alpha = 0^\circ$ and 90°, the different deformation mechanisms (extension for $\alpha = 0^\circ$ and shear for $\alpha = 90^\circ$) significantly influence the deformed shapes of the clamped–clamped and clamped–free laminates. Vel and Batra [29] used the Eshelby–Stroh formalism and obtained analytical solutions for a piezoelectric bimorph. Details of the Eshelby–Stroh formalism can be found in Ting [30]. The axis of transverse isotropy in each layer of the bimorph was not necessarily assumed to be perpendicular to the midsurface of the layer.

Here we obtain exact three-dimensional solutions for the static cylindrical bending of shear actuated hybrid laminates by the state space method. The governing equations of linear piezoelectricity simplified to the case of generalized plane strain deformation are exactly satisfied at every point in the laminate. The boundary conditions at the edges, the traction boundary conditions on the top and bottom surfaces and the continuity conditions at the interfaces between dissimilar layers are also exactly satisfied. The displacements and stresses for a homogeneous piezoelectric plate are compared with those obtained from the first-order shear deformation theory (FSDT). Hybrid laminates with a shear mode piezoelectric core sandwiched between two elastic layers are also studied. When the results are compared with those for the corresponding structure with surface-mounted extension actuators, it is seen that the longitudinal and shear stresses within the shear actuators are significantly smaller than those in the extension actuators.

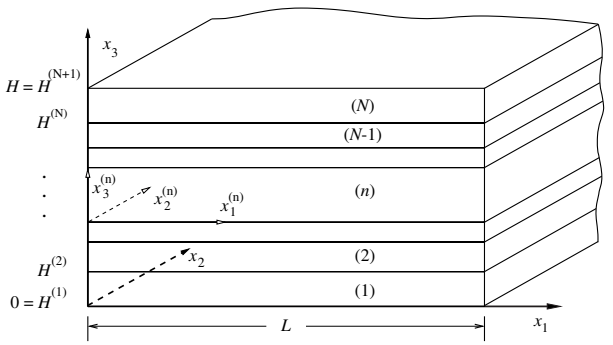

Figure 1. N-layer laminated piezoelectric plate.

Results presented herein should be useful for validating and, if necessary, refining simpler models of the system.

2. Formulation of the problem

We use a rectangular Cartesian coordinate system, shown in figure 1, to describe the infinitesimal quasistatic deformations of an N-layer piezoelectric laminated plate occupying the region $[0, L] \times (-\infty, \infty) \times [H^{(1)}, H^{(N+1)}]$ in the unstressed reference configuration. The laminate is of infinite extent in the x_2-direction. The vertical positions of the bottom and top surfaces as well as of the $N - 1$ interfaces between the adjoining laminae are denoted by $H^{(1)} = 0$, $H^{(2)}, \ldots, H^{(n)}, \ldots, H^{(N)}, H^{(N+1)} = H$. Each lamina is assumed to be made of a homogeneous material.

The equilibrium equations in the absence of body forces and free charges for the nth lamina made of a piezoelectric material are

$$\sigma^{(n)}_{jm,m} = 0 \qquad D^{(n)}_{m,m} = 0 \qquad (j, m = 1, 2, 3) \tag{1}$$

where σ_{jm} are the components of the Cauchy stress tensor and D_m the electric displacement. A comma followed by index m indicates partial differentiation with respect to the present position x_m of a material particle, a repeated index implies summation over the range of the index, and the superscript (n) signifies quantities for the nth lamina.

The elastic layers are orthotropic and the poling direction of a piezoelectric layer is in the x_1–x_2 plane. The constitutive equations for the nth lamina in contracted notation are

$$\begin{Bmatrix} \sigma_{11} \\ \sigma_{22} \\ \sigma_{33} \\ \sigma_{23} \\ \sigma_{31} \\ \sigma_{12} \end{Bmatrix}^{(n)} = \begin{bmatrix} C_{11} & C_{12} & C_{13} & 0 & 0 & C_{16} \\ C_{12} & C_{22} & C_{23} & 0 & 0 & C_{26} \\ C_{13} & C_{23} & C_{33} & 0 & 0 & C_{36} \\ 0 & 0 & 0 & C_{44} & C_{45} & 0 \\ 0 & 0 & 0 & C_{45} & C_{55} & 0 \\ C_{16} & C_{26} & C_{36} & 0 & 0 & C_{66} \end{bmatrix}^{(n)}$$
$$\times \begin{Bmatrix} \varepsilon_{11} \\ \varepsilon_{22} \\ \varepsilon_{33} \\ 2\varepsilon_{23} \\ 2\varepsilon_{31} \\ 2\varepsilon_{12} \end{Bmatrix}^{(n)} - \begin{bmatrix} e_{11} & e_{21} & 0 \\ e_{12} & e_{22} & 0 \\ e_{13} & e_{23} & 0 \\ 0 & 0 & e_{34} \\ 0 & 0 & e_{35} \\ e_{16} & e_{26} & 0 \end{bmatrix}^{(n)} \begin{Bmatrix} E_1 \\ E_2 \\ E_3 \end{Bmatrix}^{(n)}$$

$$\begin{Bmatrix} D_1 \\ D_2 \\ D_3 \end{Bmatrix}^{(n)} = \begin{bmatrix} e_{11} & e_{12} & e_{13} & 0 & 0 & e_{16} \\ e_{21} & e_{22} & e_{23} & 0 & 0 & e_{26} \\ 0 & 0 & 0 & e_{34} & e_{35} & 0 \end{bmatrix}^{(n)} \begin{Bmatrix} \varepsilon_{11} \\ \varepsilon_{22} \\ \varepsilon_{33} \\ 2\varepsilon_{23} \\ 2\varepsilon_{31} \\ 2\varepsilon_{12} \end{Bmatrix}^{(n)} + \begin{bmatrix} \epsilon_{11} & \epsilon_{12} & 0 \\ \epsilon_{12} & \epsilon_{22} & 0 \\ 0 & 0 & \epsilon_{33} \end{bmatrix}^{(n)} \begin{Bmatrix} E_1 \\ E_2 \\ E_3 \end{Bmatrix}^{(n)} \tag{2}$$

where ε_{jm} are the components of the infinitesimal strain tensor, E_j the electric field, C_{jm} the elasticity constants, e_{jm} the piezoelectric moduli and ϵ_{jm} the electric permittivity. The infinitesimal strain tensor and the electric field are related to the mechanical displacements u_j and the electric potential ϕ by

$$\varepsilon_{jm}^{(n)} = \tfrac{1}{2}(u_{j,m}^{(n)} + u_{m,j}^{(n)}) \qquad E_j^{(n)} = -\phi_{,j}^{(n)}. \tag{3}$$

The edges $x_1 = 0$ and L are assumed to be simply supported and electrically insulated; that is,

$$\sigma_{11}^{(n)} = 0 \qquad \sigma_{12}^{(n)} = 0 \qquad u_3^{(n)} = 0 \qquad D_1^{(n)} = 0 \qquad \text{at } x_1 = 0, L. \tag{4}$$

The mechanical boundary conditions of a simply supported plate characterized by the vanishing of transverse deflection and bending moments at the edges translate into the mixed boundary conditions in (4) for $\sigma_{11}^{(n)}$, $\sigma_{12}^{(n)}$ and $u_3^{(n)}$ that are identical to those assumed by Heyliger and Brooks [10] for the exact solution of simply supported plates with extension actuators. Exact three-dimensional solutions for laminated plates can be obtained only for certain combinations of boundary conditions on the edges. Heyliger and Brooks [10] assume the edges are electrically grounded ($\phi^{(n)} = 0$) in order to obtain exact solutions for laminates with piezoelectric extension actuators. In the case of piezoelectric shear actuators, we are able to obtain exact solutions only when the edges are electrically insulated ($D_1^{(n)} = 0$).

The boundary conditions prescribed on the top and bottom surfaces of the laminate are either a mechanical displacement component u_m or the corresponding traction component σ_{3m}, and either the electric potential ϕ or the normal component of the electric displacement D_3. Typically the applied traction is a normal load and the electric potential is prescribed on the surfaces. The applied pressure and the electric potential can be expanded in terms of a Fourier series. Consequently, it is sufficient to solve the problem of a laminate subjected to electrical and/or mechanical loads of the form

$$\phi(x_1, H) = \phi_0^t \cos px_1 \qquad \sigma_{33}(x_1, H) = q_0^t \sin px_1$$
$$\phi(x_1, 0) = \phi_0^b \cos px_1 \qquad \sigma_{33}(x_1, 0) = q_0^b \sin px_1 \tag{5}$$

where $\phi_0^t, q_0^t, \phi_0^b, q_0^b$ are known constants, $p = k\pi/L$ and k is a positive integer.

The interface conditions on the material surfaces $x_3 = H^{(2)}, \ldots, H^{(N)}$ may be specified as follows.

(a) If the surface $x_3 = H^{(n+1)}$ is an interface between two laminae, the mechanical displacements, surface tractions, the electric potential and the normal component of the electric displacement between them are continuous. That is

$$u_m^{(n)} = u_m^{(n+1)} \qquad \sigma_{3m}^{(n)} = \sigma_{3m}^{(n+1)} \qquad \phi^{(n)} = \phi^{(n+1)} \qquad D_3^{(n)} = D_3^{(n+1)} \qquad \text{on } x_3 = H^{(n+1)}. \tag{6}$$

Thus the adjoining laminae are presumed to be mechanically and electrically perfectly bonded together.

(b) If the interface $x_3 = H^{(n+1)}$ is electroded, then the potential on this surface is assumed to be a known function of the form $\phi_0^{(n+1)} \cos px_1$. The normal component of the electric displacement need not be continuous across this interface. Thus

$$u_m^{(n)} = u_m^{(n+1)} \qquad \sigma_{3m}^{(n)} = \sigma_{3m}^{(n+1)}$$
$$\phi^{(n)} = \phi^{(n+1)} = \phi_0^{(n+1)} \cos px_1 \qquad \text{on } x_3 = H^{(n+1)}. \tag{7}$$

3. Exact solution

We construct a local coordinate system $x_1^{(n)}, x_2^{(n)}, x_3^{(n)}$ with the local axes parallel to the global axes and the origin at the point where the global x_3-axis intersects the bottom surface of the nth lamina (see figure 1). In this local coordinate system, the nth lamina occupies the region $[0, L] \times (-\infty, \infty) \times [0, h^{(n)}]$, where $h^{(n)} = H^{(n+1)} - H^{(n)}$. We postulate that the displacements $u_k^{(n)}$ and the electric potential $\phi^{(n)}$ are functions of x_1 and x_3 only. Thus the laminate is in a generalized plane state of deformation. This assumption is reasonable because the applied loads (mechanical and/or electrical) and material properties are independent of x_2, and the body is of infinite extent in the x_2-direction.

A solution for displacement components and the electric potential for the nth lamina is sought in the form

$$\begin{aligned} u_1^{(n)}(x_1^{(n)}, x_3^{(n)}) &= U_1^{(n)}(x_3^{(n)}) \cos px_1^{(n)} \\ u_2^{(n)}(x_1^{(n)}, x_3^{(n)}) &= U_2^{(n)}(x_3^{(n)}) \cos px_1^{(n)} \\ u_3^{(n)}(x_1^{(n)}, x_3^{(n)}) &= U_3^{(n)}(x_3^{(n)}) \sin px_1^{(n)} \\ \phi^{(n)}(x_1^{(n)}, x_3^{(n)}) &= \Phi^{(n)}(x_3^{(n)}) \cos px_1^{(n)}. \end{aligned} \tag{8}$$

Equations (8) identically satisfy the homogeneous boundary conditions (4) on the edges $x_1 = 0$ and L.

Substitution of (8) into (3) and the result into (2) gives the following expressions for the stresses and electric displacements

$$\begin{aligned} \sigma_{11}^{(n)} &= (-C_{11}^{(n)} U_1^{(n)} p + C_{13}^{(n)} U_{3,3}^{(n)} - C_{16}^{(n)} U_2^{(n)} p \\ &\quad - e_{11}^{(n)} \Phi^{(n)} p) \sin px_1^{(n)} \\ \sigma_{22}^{(n)} &= (-C_{12}^{(n)} U_1^{(n)} p + C_{23}^{(n)} U_{3,3}^{(n)} - C_{26}^{(n)} U_2^{(n)} p \\ &\quad - e_{12}^{(n)} \Phi^{(n)} p) \sin px_1^{(n)} \\ \sigma_{33}^{(n)} &= (-C_{13}^{(n)} U_1^{(n)} p + C_{33}^{(n)} U_{3,3}^{(n)} - C_{36}^{(n)} U_2^{(n)} p \\ &\quad - e_{13}^{(n)} \Phi^{(n)} p) \sin px_1^{(n)} \\ \sigma_{23}^{(n)} &= (C_{44}^{(n)} U_{2,3}^{(n)} + C_{45}^{(n)} U_{1,3}^{(n)} + C_{45}^{(n)} U_3^{(n)} p \\ &\quad + e_{34}^{(n)} \Phi_{,3}^{(n)}) \cos px_1^{(n)} \\ \sigma_{31}^{(n)} &= (C_{45}^{(n)} U_{2,3}^{(n)} + C_{55}^{(n)} U_{1,3}^{(n)} + C_{55}^{(n)} U_3^{(n)} p \\ &\quad + e_{35}^{(n)} \Phi_{,3}^{(n)}) \cos px_1^{(n)} \\ \sigma_{12}^{(n)} &= (-C_{16}^{(n)} U_1^{(n)} p + C_{36}^{(n)} U_{3,3}^{(n)} - C_{66}^{(n)} U_2^{(n)} p \\ &\quad - e_{16}^{(n)} \Phi^{(n)} p) \sin px_1^{(n)} \end{aligned}$$

$$
\begin{aligned}
D_1^{(n)} &= (-e_{11}^{(n)} U_1^{(n)} p + e_{13}^{(n)} U_{3,3}^{(n)} - e_{16}^{(n)} U_2^{(n)} p \\
&\quad + \epsilon_{11}^{(n)} \Phi^{(n)} p) \sin p x_1^{(n)} \\
D_2^{(n)} &= (-e_{21}^{(n)} U_1^{(n)} p + e_{23}^{(n)} U_{3,3}^{(n)} - e_{26}^{(n)} U_2^{(n)} p \\
&\quad + \epsilon_{12}^{(n)} \Phi^{(n)} p) \sin p x_1^{(n)} \\
D_3^{(n)} &= (e_{34}^{(n)} U_{2,3}^{(n)} + e_{35}^{(n)} U_{1,3}^{(n)} + e_{35}^{(n)} U_3^{(n)} p \\
&\quad - \epsilon_{33}^{(n)} \Phi_{,3}^{(n)}) \cos p x_1^{(n)}.
\end{aligned} \tag{9}
$$

Substitution of (9) into the governing equations (1), and writing the resulting system of second-order differential equations as a set of first-order differential equations, we obtain the following state space matrix equation

$$
\mathbf{K}^{(n)} \mathbf{Y}_{,3}^{(n)} = \mathbf{A}^{(n)} \mathbf{Y}^{(n)} \tag{10}
$$

where $\mathbf{Y}^{(n)}$ is a 8×1 vector of variables defined as

$$
\begin{aligned}
&Y_1^{(n)} = U_1^{(n)} \qquad Y_2^{(n)} = U_2^{(n)} \qquad Y_3^{(n)} = U_3^{(n)} \\
&Y_4^{(n)} = \Phi^{(n)} \qquad Y_5^{(n)} = U_{1,3}^{(n)} \qquad Y_6^{(n)} = U_{2,3}^{(n)} \\
&\qquad Y_7^{(n)} = U_{3,3}^{(n)} \qquad Y_8^{(n)} = \Phi_{,3}^{(n)}
\end{aligned} \tag{11}
$$

and the 8×8 matrices $\mathbf{K}^{(n)}$ and $\mathbf{A}^{(n)}$ are

$$
\mathbf{K}^{(n)} = \begin{bmatrix}
1 & 0 & 0 & 0 & 0 & 0 & 0 & 0 \\
0 & 1 & 0 & 0 & 0 & 0 & 0 & 0 \\
0 & 0 & 1 & 0 & 0 & 0 & 0 & 0 \\
0 & 0 & 0 & 1 & 0 & 0 & 0 & 0 \\
0 & 0 & 0 & 0 & C_{55}^{(n)} & C_{45}^{(n)} & 0 & e_{35}^{(n)} \\
0 & 0 & 0 & 0 & C_{45}^{(n)} & C_{44}^{(n)} & 0 & e_{34}^{(n)} \\
0 & 0 & 0 & 0 & 0 & 0 & C_{33}^{(n)} & 0 \\
0 & 0 & 0 & 0 & -e_{35}^{(n)} & -e_{34}^{(n)} & 0 & \epsilon_{33}^{(n)}
\end{bmatrix}
$$

$$
\mathbf{A}^{(n)} = \begin{bmatrix}
0 & 0 & 0 & 0 \\
0 & 0 & 0 & 0 \\
0 & 0 & 0 & 0 \\
0 & 0 & 0 & 0 \\
C_{11}^{(n)} p^2 & C_{16}^{(n)} p^2 & 0 & e_{11}^{(n)} p^2 \\
C_{16}^{(n)} p^2 & C_{66}^{(n)} p^2 & 0 & e_{16}^{(n)} p^2 \\
0 & 0 & C_{55}^{(n)} p^2 & 0 \\
-e_{11}^{(n)} p^2 & -e_{16}^{(n)} p^2 & 0 & \epsilon_{11}^{(n)} p^2
\end{bmatrix}
\begin{bmatrix}
1 & 0 & 0 \\
0 & 1 & 0 \\
0 & 0 & 1 \\
0 & 0 & 0 \\
0 & 0 & -(C_{13}^{(n)} + C_{55}^{(n)}) p \\
0 & 0 & -(C_{36}^{(n)} + C_{45}^{(n)}) p \\
(C_{13}^{(n)} + C_{55}^{(n)}) p & (C_{36}^{(n)} + C_{45}^{(n)}) p & 0 \\
0 & 0 & (e_{35}^{(n)} + e_{13}^{(n)}) p
\end{bmatrix}
\begin{bmatrix}
0 \\ 0 \\ 0 \\ 1 \\ 0 \\ 0 \\ 0 \\ (e_{35}^{(n)} + e_{13}^{(n)}) p
\end{bmatrix}
\begin{bmatrix}
0 \\ 0 \\ 0 \\ 0 \\ 1 \\ 0 \\ 0 \\ 0
\end{bmatrix}. \tag{12}
$$

The solution of (10) is

$$
\mathbf{Y}^{(n)}(x_3^{(n)}) = \exp[(\mathbf{K}^{(n)})^{-1} \mathbf{A}^{(n)} x_3^{(n)}] \mathbf{Z}^{(n)} \tag{13}
$$

where $\mathbf{Z}^{(n)}$ is an 8×1 vector of unknown coefficients. The matrix exponential in (13) is obtained by using Mathematica [31] via the Jordan decomposition of $(\mathbf{K}^{(n)})^{-1} \mathbf{A}^{(n)}$. We thus obtain analytical expressions for functions $U_j^{(n)}$ and $\Phi^{(n)}$ in terms of eight scalar coefficients $Z_m^{(n)}$, $m = 1, 2, \ldots, 8$, for each lamina. The coefficients are determined by satisfying the boundary conditions on the top and bottom surfaces of the laminate as well as the interface conditions (6) or (7) between adjoining dissimilar plies. This results in four conditions on both the top and bottom surfaces and eight conditions at each of the $(N-1)$ interfaces. The resulting system of $8N$ linear algebraic equations for the $8N$ unknowns $Z_m^{(n)} (n = 1, 2, \ldots, N)$ is readily solved. Once the constants are determined, the mechanical displacements, stresses, electric potential and electric displacement can be computed at any location within the laminate.

4. FSDT solution

Consider a homogeneous plate of thickness H made of a piezoelectric material whose poling direction is in the x_1–x_2 plane. The edges are simply supported and the top and bottom surfaces are subjected to the following mechanical and electric loads

$$
\begin{aligned}
&\sigma_{33}(x_1, H) = q_0 \sin \frac{\pi x_1}{L} \qquad \phi(x_1, H) = \phi_0 \cos \frac{\pi x_1}{L} \\
&\sigma_{33}(x_1, 0) = 0 \qquad \phi(x_1, 0) = 0
\end{aligned} \tag{14}
$$

where ϕ_0 and q_0 are known constants. We take the bottom surface of the plate as the reference surface and assume the following fields for the displacements and the electric potential

$$
\begin{aligned}
u_1(x_1, x_3) &= u_1^0(x_1) + x_3 \varphi_1(x_1) \\
u_2(x_1, x_3) &= u_2^0(x_1) + x_3 \varphi_2(x_1) \\
u_3(x_1, x_3) &= u_3^0(x_1), \quad \phi = \phi_0 \frac{x_3}{H} \cos \frac{\pi x_1}{L}.
\end{aligned} \tag{15}
$$

Here $u_k^0(x_1)$ are the displacements of a point on the bottom surface, and $\varphi_1(x_1)$ and $-\varphi_2(x_1)$ are the rotations of the transverse normal to the bottom surface about the x_2- and x_1-axes, respectively. The non-zero infinitesimal strains and the components of the electric field associated with (15) are

$$
\begin{aligned}
&\varepsilon_{11} = \frac{\mathrm{d}u_1^0}{\mathrm{d}x_1} + x_3 \frac{\mathrm{d}\varphi_1}{\mathrm{d}x_1} \qquad 2\varepsilon_{23} = \varphi_2 \qquad 2\varepsilon_{13} = \frac{\mathrm{d}u_3^0}{\mathrm{d}x_1} + \varphi_1 \\
&2\varepsilon_{12} = \frac{\mathrm{d}u_2^0}{\mathrm{d}x_1} + x_3 \frac{\mathrm{d}\varphi_2}{\mathrm{d}x_1} \qquad E_1 = \phi_0 \frac{\pi x_3}{LH} \sin \frac{\pi x_1}{L} \\
&E_3 = -\frac{\phi_0}{H} \cos \frac{\pi x_1}{L}.
\end{aligned} \tag{16}
$$

The following reduced stress–strain relationship (17) is obtained by setting $\sigma_{33} = 0$ in equation (2). From this assumption, ε_{33} is computed in terms of ε_{11}, ε_{22}, ε_{12}, E_1 and E_3 and then substituted into the expressions for σ_{11}, σ_{22}, σ_{23}, σ_{13} and σ_{12} in (2). A limitation of the FSDT is that both σ_{33} and ε_{33} are assumed to vanish; this has been corrected in the plate theory proposed by Vidoli and Batra [28]. In the FSDT the through-thickness variation of σ_{33} is computed by integrating

Table 1. Non-vanishing material properties of the graphite-epoxy and PZT-5A shear actuators.

Property	0° graphite-epoxy	±45° graphite-epoxy	0° PZT-5A	45° PZT-5A
C_{11} (GPa)	183.443	58.128	86.856	93.003
C_{22} (GPa)	11.662	58.128	99.201	93.003
C_{33} (GPa)	11.662	11.662	99.201	99.201
C_{12} (GPa)	4.363	43.788	50.778	50.803
C_{13} (GPa)	4.363	4.140	50.778	52.397
C_{23} (GPa)	3.918	4.140	54.016	52.397
C_{44} (GPa)	2.870	5.020	22.593	21.847
C_{55} (GPa)	7.170	5.020	21.100	21.847
C_{66} (GPa)	7.170	46.595	21.100	21.126
C_{16} (GPa)	0	±42.945	0	−3.086
C_{26} (GPa)	0	±42.945	0	−3.086
C_{36} (GPa)	0	±0.222	0	−1.619
C_{45} (GPa)	0	±2.150	0	−0.7465
e_{11} (C m^{-2})	0	0	15.118	11.510
e_{12} (C m^{-2})	0	0	−7.209	−5.917
e_{13} (C m^{-2})	0	0	−7.209	−5.098
e_{16} (C m^{-2})	0	0	0	7.894
e_{21} (C m^{-2})	0	0	0	−5.917
e_{22} (C m^{-2})	0	0	0	11.510
e_{23} (C m^{-2})	0	0	0	−5.098
e_{26} (C m^{-2})	0	0	12.322	7.894
e_{34} (C m^{-2})	0	0	0	8.713
e_{35} (C m^{-2})	0	0	12.322	8.713
ϵ_{11} (10^{-10} F m^{-1})	153.0	153.0	150.0	151.5
ϵ_{22} (10^{-10} F m^{-1})	153.0	153.0	153.0	151.5
ϵ_{33} (10^{-10} F m^{-1})	153.0	153.0	153.0	153.0
ϵ_{12} (10^{-10} F m^{-1})	0	0	0	−1.50

the equilibrium equations in the thickness direction. Since $\varepsilon_{22} = 0$, the reduced stress–strain relationship is written as

$$\begin{Bmatrix} \sigma_{11} \\ \sigma_{23} \\ \sigma_{13} \\ \sigma_{12} \end{Bmatrix} = \begin{bmatrix} \bar{Q}_{11} & 0 & 0 & \bar{Q}_{16} & -\bar{e}_{11} & 0 \\ 0 & \bar{Q}_{44} & \bar{Q}_{45} & 0 & 0 & -\bar{e}_{34} \\ 0 & \bar{Q}_{45} & \bar{Q}_{55} & 0 & 0 & -\bar{e}_{35} \\ \bar{Q}_{16} & 0 & 0 & \bar{Q}_{66} & -\bar{e}_{16} & 0 \end{bmatrix} \times \begin{Bmatrix} \varepsilon_{11} \\ 2\varepsilon_{23} \\ 2\varepsilon_{13} \\ 2\varepsilon_{12} \\ E_1 \\ E_3 \end{Bmatrix} \tag{17}$$

where

$$\bar{Q}_{11} = C_{11} - \frac{C_{13}^2}{C_{33}} \qquad \bar{Q}_{16} = C_{16} - \frac{C_{13}C_{36}}{C_{33}}$$

$$\bar{e}_{11} = e_{11} - \frac{C_{13}e_{13}}{C_{33}}$$

$$\bar{Q}_{44} = C_{44} \qquad \bar{Q}_{45} = C_{45} \qquad \bar{Q}_{55} = C_{55}$$

$$\bar{e}_{34} = e_{34} \qquad \bar{e}_{35} = e_{35}$$

$$\bar{Q}_{66} = C_{66} - \frac{C_{36}^2}{C_{33}} \qquad \bar{e}_{16} = e_{16} - \frac{C_{36}e_{13}}{C_{33}}. \tag{18}$$

The variational principle for a piezoelectric medium (e.g. see Tiersten [32]) gives the following governing equations

$$\frac{\mathrm{d}N_{11}}{\mathrm{d}x_1} = 0 \qquad \frac{\mathrm{d}N_{12}}{\mathrm{d}x_1} = 0 \qquad \frac{\mathrm{d}Q_1}{\mathrm{d}x_1} + q_0 \sin\frac{\pi x_1}{L} = 0$$

$$\frac{\mathrm{d}M_{11}}{\mathrm{d}x_1} - Q_1 = 0 \qquad \frac{\mathrm{d}M_{12}}{\mathrm{d}x_1} - Q_2 = 0 \tag{19}$$

with the stress resultants defined as

$$[N_{11}, M_{11}] = \int_0^H \sigma_{11}[1, x_3]\,\mathrm{d}x_3$$

$$[N_{12}, M_{12}] = \int_0^H \sigma_{12}[1, x_3]\,\mathrm{d}x_3$$

$$[Q_1, Q_2] = \int_0^H \mathcal{K}[\sigma_{13}, \sigma_{23}]\,\mathrm{d}x_3. \tag{20}$$

The charge equation $(1)_2$ has not been considered in the derivation of the equilibrium equations (19) because the electric potential has been assumed *a priori*. Thus there is no contribution from the electric internal virtual work term $\int D_i \delta E_i$ in the variational statement. The constant $\mathcal{K}$ is the shear correction coefficient that is set equal to 5/6 as proposed by Mindlin and Reissner for a homogenous elastic plate. It should be noted that σ_{22}, although non-zero, is omitted from the reduced constitutive relationship (17) since the stress resultant N_{22} does not appear in the governing equations (19). The normal stress σ_{22} can be computed from the constitutive equations after a solution has been obtained for the displacements.

In the FSDT, the boundary conditions for simply supported edges are written as

$$N_{11} = N_{12} = 0 \qquad M_{11} = M_{12} = 0 \qquad u_3^0 = 0$$
$$\text{at } x_1 = 0 \text{ and } L. \tag{21}$$

The electric boundary condition $D_1 = 0$ is identically satisfied at the edges $x_1 = 0$ and L by our choice for the mechanical displacements and electric potential in (15). A solution to the

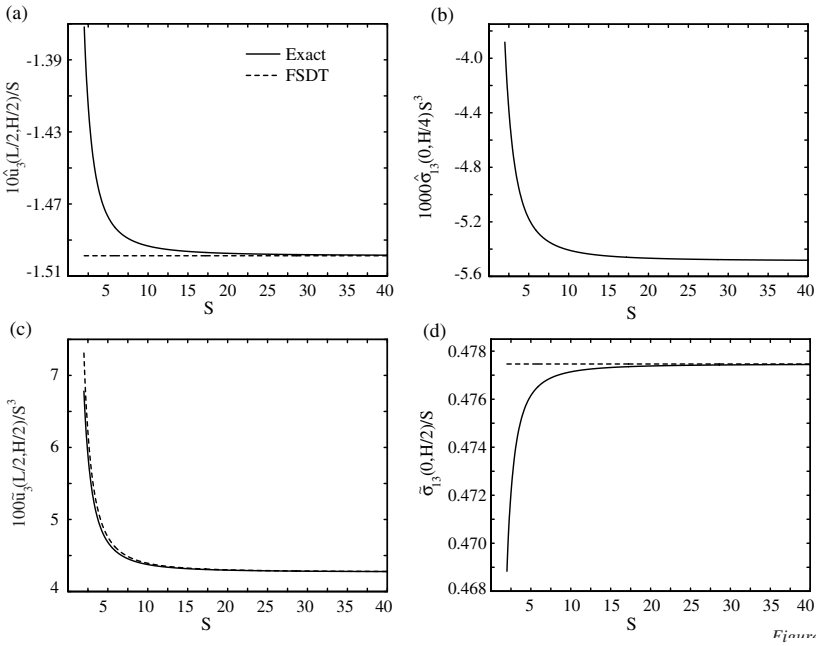

Figure 2. Transverse deflection and transverse shear stress for a homogeneous 0° PZT-5A plate versus length-to-thickness ratio S: (a, b) electric load and (c, d) mechanical load.

ordinary differential equations (19) is obtained by choosing the displacements and rotations as

$$[u_1^0(x_1), u_2^0(x_1), \varphi_1(x_1), \varphi_2(x_1)] = [R_1, R_2, R_3, R_4]\cos\frac{\pi x_1}{L}$$

$$u_3^0(x_1) = R_5 \sin\frac{\pi x_1}{L}. \tag{22}$$

These satisfy the edge conditions (21) identically. Substitution from (22) into (16) and the result into (17) gives stresses in terms of ϕ_0 and the unknowns $R_k, k = 1, \ldots, 5$. The expressions for the stresses are then substituted into (20) and for the stress resultants into (19) to obtain five simultaneous linear equations for the five unknowns R_k, which can be readily solved. When the poling direction coincides with the x_1-axis, the solution for the displacements and stresses under combined mechanical and electrical loads are

$$u_1(x_1, x_3) = -\left[\frac{\bar{e}_{11}}{\bar{Q}_{11}}\frac{x_3}{H}\phi_0 + \frac{6LS^2}{\pi^3\bar{Q}_{11}}\left(2\frac{x_3}{H} - 1\right)q_0\right]\cos\frac{\pi x_1}{L} \qquad u_2(x_1, x_3) = 0$$

$$u_3(x_1, x_3) = \left[\left(\frac{\bar{e}_{11}}{\pi\bar{Q}_{11}} - \frac{\bar{e}_{35}}{\pi\bar{Q}_{55}}\right)S\phi_0 + \left(\frac{1}{\pi^2\mathcal{K}\bar{Q}_{55}} + \frac{12S^2}{\pi^4\bar{Q}_{11}}\right)SLq_0\right]\sin\frac{\pi x_1}{L}$$

$$\sigma_{11}(x_1, x_3) = \frac{6S^2q_0}{\pi^2}\left(\frac{2x_3}{H} - 1\right)\sin\frac{\pi x_1}{L}$$

$$\sigma_{13}(x_1, x_3) = -\frac{6Sq_0}{\pi}\left(\frac{x_3}{H} - 1\right)\frac{x_3}{H}\cos\frac{\pi x_1}{L}$$

$$\sigma_{12}(x_1, x_3) = \sigma_{23}(x_1, x_3) = 0 \tag{23}$$

where $S = L/H$ is the length-to-thickness ratio of the plate. If the poling direction is inclined at an angle to the x_1-axis, then the expressions for the displacements and stresses are more complicated and are omitted for the sake of brevity. For the FSDT solution, the transverse shear stresses σ_{13} and σ_{23} are obtained by integrating the three-dimensional equilibrium equations in the thickness direction.

5. Results and discussion

We present results for hybrid laminates with each lamina made of either graphite-epoxy or PZT-5A. The principal axis of the graphite-epoxy lamina is assumed to be in the x_1–x_2 plane and inclined at an angle ψ to the x_1-axis. If the poling direction of PZT-5A is inclined at an angle of θ degrees to the x_1-axis on the x_1–x_2 plane, we denote it as θ° PZT-5A. The material properties for the θ° PZT-5A (including $\theta = 0$) are obtained by a tensor transformation of the material properties given by Tang *et al* [33] of PZT-5A poled in the x_3-direction; these should be representative of θ° PZTs. The authors are not aware of test data for PZTs poled in the axial direction. The non-zero values of the material properties are listed in table 1 for $\psi = 0^\circ$, $\psi = \pm 45^\circ$, $\theta = 0^\circ$ and $\theta = 45^\circ$.

5.1. Homogeneous piezoelectric plate

Consider a single homogeneous layer of 0° PZT-5A subjected to the sinusoidal electric and/or mechanical load (14) on the top and bottom surfaces. The displacements and stresses are non-dimensionalized as

$$\hat{u}_k = u_k C_0/e_0\phi_0 \qquad \hat{\sigma}_{ij} = \sigma_{ij}L/e_0\phi_0$$

for the applied electric load and

$$\tilde{u}_k = u_k C_0/Lq_0 \qquad \tilde{\sigma}_{ij} = \sigma_{ij}/q_0$$

for the applied mechanical load. Here $C_0 = 21.1$ GPa and $e_0 = 12.322$ C m^{-2} are representative values of the elastic and piezoelectric moduli, respectively for PZT-5A. The FSDT

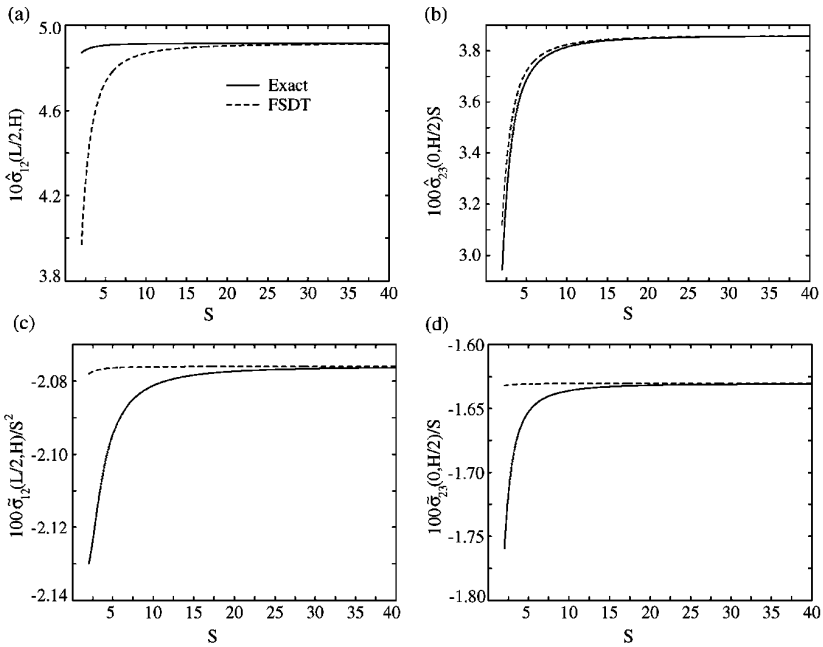

Figure 3. Stresses in a homogeneous 45° PZT-5A plate versus length-to-thickness ratio: (a, b) electric load and (c, d) mechanical load.

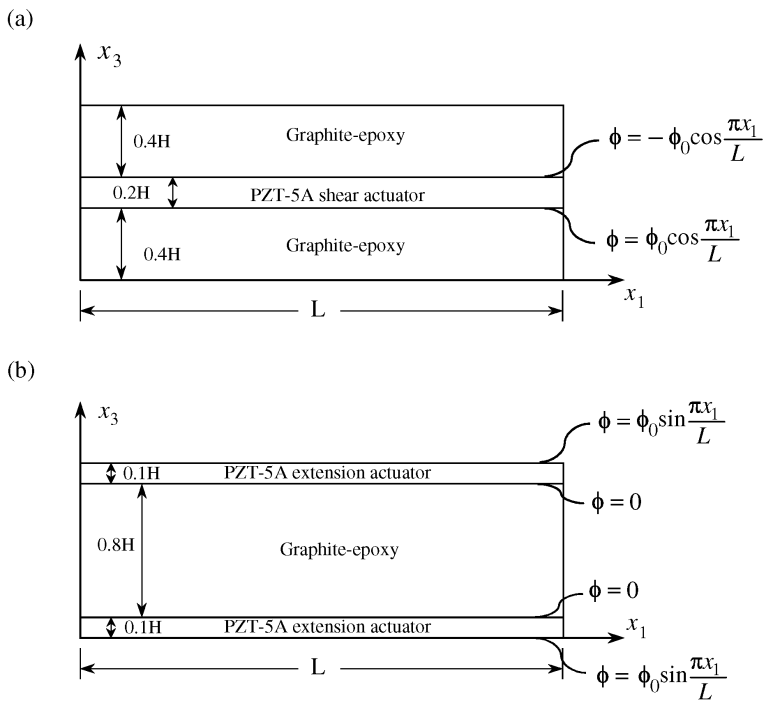

Figure 4. (a) Axially poled piezoelectric shear actuator core sandwiched between graphite-epoxy facing sheets and (b) corresponding extension actuation configuration with transversely poled actuators.

solution is compared with the exact solution in figure 2 for length-to-thickness ratios, S, from 2 to 40. The midpoint transverse deflection $\hat{u}_3(L/2, H/2)$ predicted by the FSDT for the electric load is in good agreement with the exact solution for $S > 10$ as depicted in figure 2(a). The FSDT predicts the transverse shear stress $\hat{\sigma}_{13}$ to be zero for the electric load. The exact solution gives a non-zero, but small value for $\hat{\sigma}_{13}$ that is inversely proportional to S^3 for $S \geqslant 15$ (figure 2(b)). As shown in figures 2(c) and 2(d) for a mechanical load, the midpoint transverse deflection $\tilde{u}_3$ and the transverse shear stress $\tilde{\sigma}_{13}$ computed from the FSDT are in excellent agreement with those obtained from the exact solution even for thick plates ($S < 10$). Note that the vertical scale in figure 2(d) has been significantly magnified.

The stresses at two locations in a homogeneous piezoelectric plate with the poling direction inclined at 45° to the x_1-axis (i.e. 45° PZT-5A) are depicted in figure 3. For the electric load, the in-plane shear stress $\hat{\sigma}_{12}$ from the FSDT compares well with that computed from the exact solution for $S > 10$, and the two values of the transverse shear stress $\hat{\sigma}_{23}$

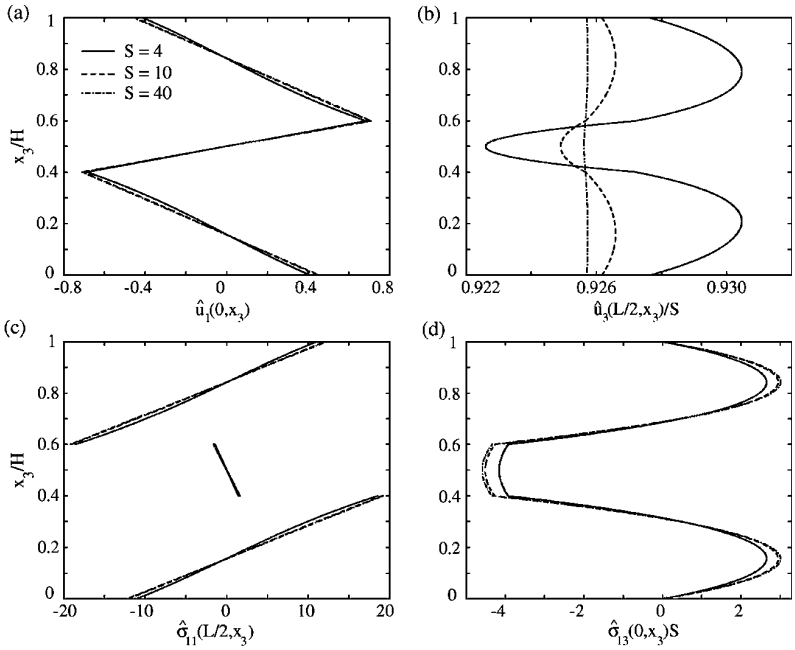

Figure 5. Through-thickness distribution of displacements and stresses for a shear piezoelectric actuator sandwiched between graphite-epoxy facing sheets and subjected to an electric load.

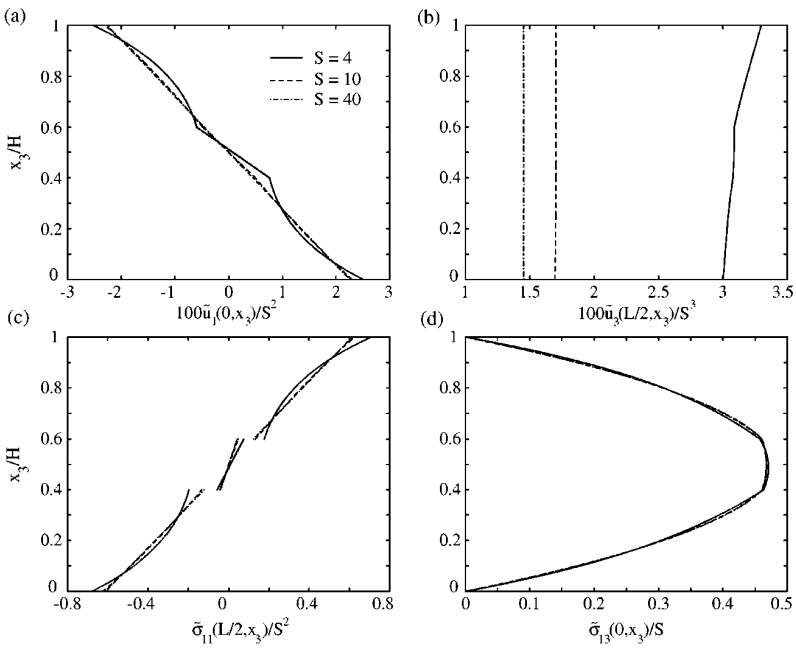

Figure 6. Through-thickness distribution of displacements and stresses for a shear piezoelectric actuator sandwiched between graphite-epoxy facing sheets and subjected to a mechanical load.

are in good agreement with each other even for thick plates (figures 3(a) and 3(b)). For the mechanical load, the stresses $\tilde{\sigma}_{12}$ and $\tilde{\sigma}_{23}$ from the FSDT and the exact solution shown in figures 3(c) and 3(d) agree well with each other for $S > 10$.

5.2. Hybrid laminate with a piezoelectric core

As shown in figure 4(a), we consider a hybrid laminate with the top and bottom layers made of 0° graphite-epoxy and the central layer made of 0° PZT-5A with electroded top and bottom surfaces. Application of electric potentials $-\phi_0 \cos \pi x_1/L$ and $\phi_0 \cos \pi x_1/L$ to the top and bottom surfaces, respectively, of the piezoelectric core will produce a transverse shear deformation that will deflect the laminate in the transverse direction. The through-thickness variations of the exact displacements and stresses for length-to-thickness ratios $S = 4, 10$ and 40 are depicted in figure 5. The axial displacement $\hat{u}_1$ is 'zig–zag' shaped for thick as well as thin laminates (figure 5(a)). This implies that an equivalent-single-layer theory, like the FSDT, that assumes an affine variation for the displacements through the entire thickness of the laminate will yield poor results even for a thin sandwich

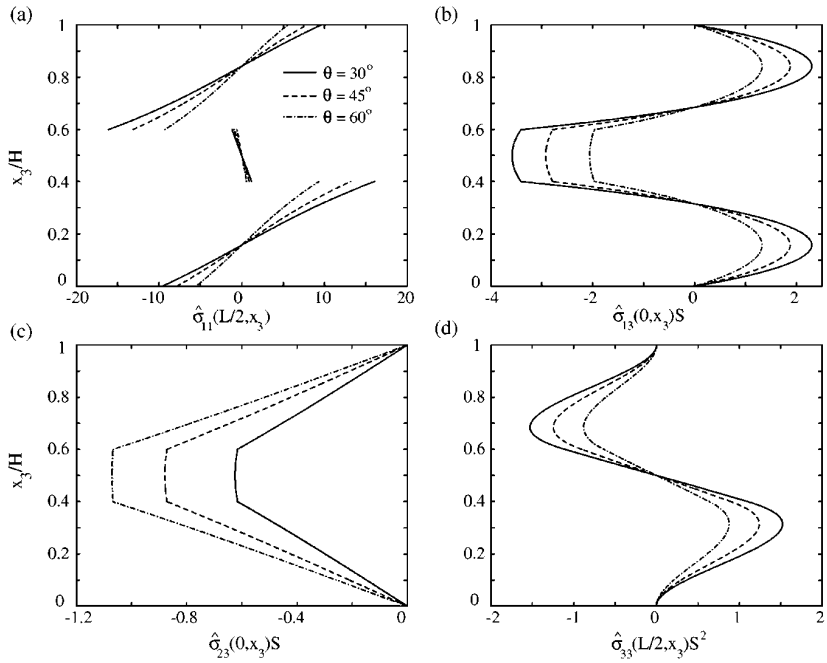

Figure 7. Comparison of through-thickness distribution of stresses for 30°, 45° and 60° PZT-5A shear piezoelectric actuators sandwiched between 0° graphite-epoxy facing sheets and subjected to an electrical load, $S = 4$.

laminate. If the hybrid structure contains a piezoelectric core, then a layerwise theory must be used even for thin laminates. Zhang and Sun [21] developed a layerwise theory for sandwich structures with a piezoelectric core. They treat the top and bottom elastic sheets as Euler–Bernoulli beams and the piezoelectric core as a Timoshenko beam. The exact transverse displacement approaches a constant value through the entire thickness for large values of S as shown in figure 5(b). The longitudinal stress is piecewise affine through the thickness and is significantly smaller in the piezoelectric core than that in the graphite-epoxy layers (figure 5(c)). The transverse shear stress shown in figure 5(d) attains its maximum value at the centre of the piezoelectric core.

Figure 6 depicts the displacements and stresses in the laminate subjected only to the sinusoidal mechanical load $\sigma_{33}(x_1, H) = q_0 \sin \pi x_1/L$ on its top surface. The through-thickness variation of the axial displacement approaches an affine distribution for increasing length-to-thickness ratios (figure 6(a)). As shown in figure 6(b), the top surface of a thick laminate exhibits a larger transverse deflection than the bottom surface, while it approaches a constant value for all points along the thickness for a thin laminate. The average transverse normal strain $\varepsilon_{33}C_0/q_0$ at midspan remains the same for thick and thin laminates and equals 0.755, 0.756 and 0.756 for $S = 4$, 10 and 40, respectively. The normalized midpoint transverse deflection is larger for thick laminates than that for thin laminates due to the effect of shear deformation. The longitudinal stress in the piezoelectric core is smaller than that in the graphite-epoxy layers, as one would expect, since it is closer to the midplane (figure 6(c)). The through-thickness variation of the transverse shear stress is depicted in figure 6(d).

Consider the sandwich structure shown in figure 4(a) with a θ° PZT-5A core sandwiched between 0° graphite-epoxy layers. The through-thickness distribution of the stresses for angles $\theta = 30^\circ, 45^\circ$ and 60° are shown in figure 7 for

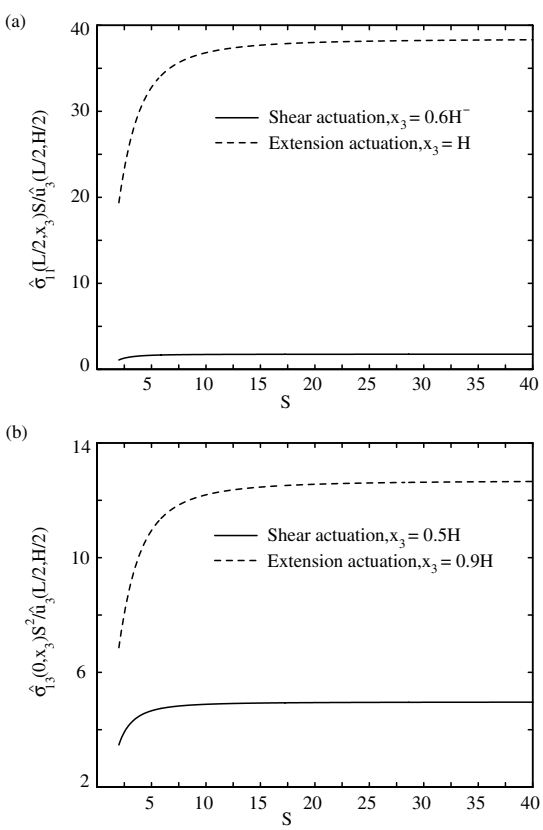

Figure 8. Comparison of the stresses in the piezoelectric layer for a shear actuation mechanism and the corresponding extension actuation mechanism for an electric load: (a) longitudinal stress and (b) transverse shear stress.

$S = 4$. While the magnitudes of the stresses depend on the poling direction θ of the PZT core, the shapes of the curves

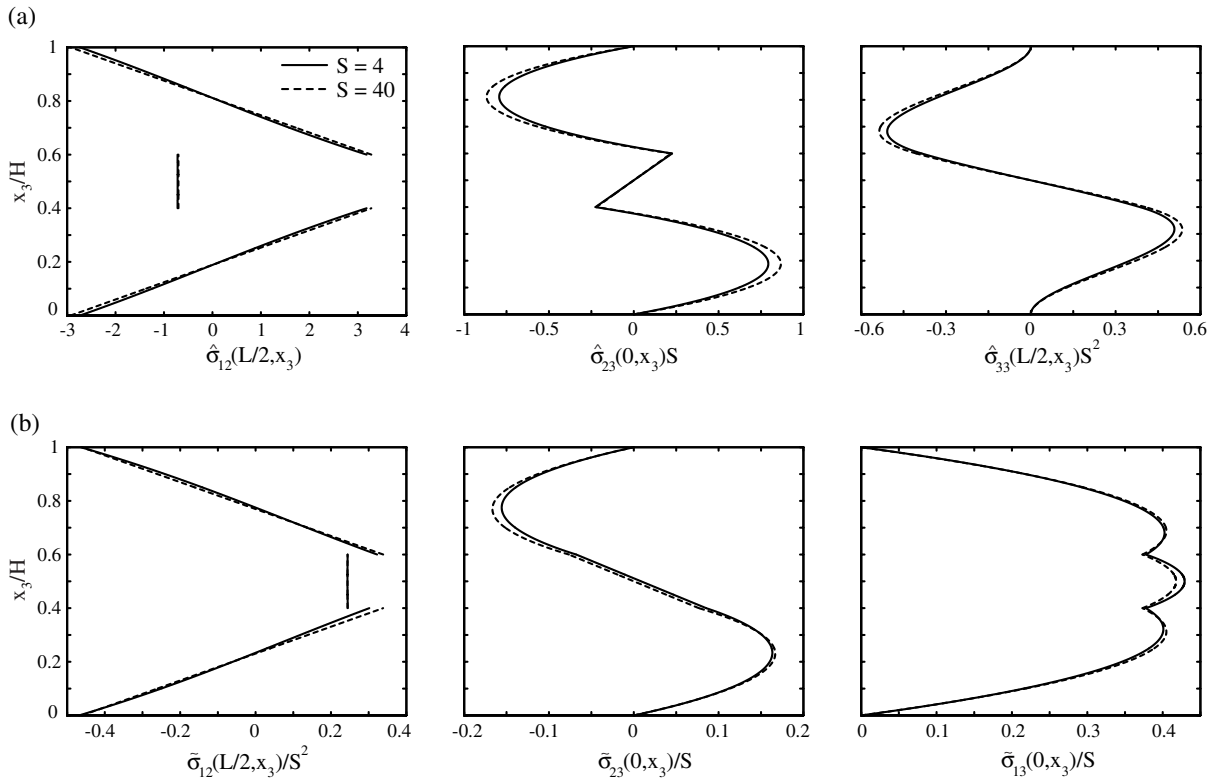

Figure 9. Stresses in a three-ply laminate for a 0° PZT-5A shear actuator sandwiched between a 45° graphite-epoxy facing sheet at the bottom and a −45° graphite-epoxy facing sheet at the top: (*a*) electrical load and (*b*) mechanical load.

remain unchanged. As θ increases, the magnitude of the transverse shear stress $\hat{\sigma}_{13}$ decreases and $\hat{\sigma}_{23}$ increases since the piezoelectric coefficient e_{35} of the core becomes smaller and e_{34} becomes larger.

Zhang and Sun [21] performed a comparative study of two cantilever beams similar to those shown in figure 4. They observe that the greatest advantage provided by the sandwich beam with a piezoelectric core is that stresses induced in the PZT layer are lower than those in the other beam. Since we have obtained the exact solution for shear actuators, and the exact solution for the extension actuation mechanism was given by Heyliger and Brooks [10], we can compare the stresses induced in the PZT used in the two configurations shown in figure 4 when the edges are simply supported. The piezoelectric actuators in figure 4(*b*) are poled in the x_3-direction. The combined thickness of the two piezoelectric actuators and the applied electric field intensity are the same as those for the shear actuation configuration of figure 4(*a*). The longitudinal stress in the piezoelectric actuator divided by the transverse deflection versus S is shown in figure 8(*a*) for the two configurations. The thickness location at which the longitudinal stresses are compared are different since the maximum longitudinal stress in the shear actuator occurs at $x_3 = 0.6H^-$ (and $0.4H^+$) while it occurs at $x_3 = H$ (and 0) for the extension actuators. We use $H^{\pm}$, defined as $\lim_{\delta\to 0} H \pm \delta$, since the longitudinal stress may be discontinuous across the interface between laminae. As is evident, the longitudinal stress in the shear actuator is significantly smaller than that in the extension actuator to achieve a given transverse deflection of the plate. This is advantageous since a large longitudinal tensile stress is detrimental to the brittle piezoceramic material. The transverse shear stress in the piezoelectric material is maximum on the interface $x_3 = 0.9H$ for extension actuators. For shear actuators, the transverse shear stress is largest at the midsurface $x_3 = 0.5H$. A comparison of the transverse shear stresses at these locations for the two configurations is shown in figure 8(*b*) for various length-to-thickness ratios. These plots reveal that the maximum transverse shear stress is also smaller for shear actuators than that for extension actuators. Thus our comparison of the exact results for the two configurations support the conclusions of Zhang and Sun [21]. It should be noted that Heyliger and Brooks [10] have considered grounded edges and sinusoidal electric load for extension actuators whereas we have assumed electrically insulated edges and co-sinusoidal loads to obtain exact solutions for shear actuators. In spite of these differences, the results presented in this section provide a useful comparison of the effectiveness of extension and shear actuators.

As a final example we consider the sandwich structure shown in figure 4(*a*) with the bottom and top layers made of graphite-epoxy with principal directions oriented at 45° and −45°, respectively, to the x_1-axis. The central layer is a 0° PZT-5A piezoelectric core. The thicknesses of the laminae and the electric potential applied to the core are the same as shown in figure 4(*a*). Figure 9(*a*) depicts the through-thickness variation of the in-plane shear stress $\hat{\sigma}_{12}$, the transverse shear stress $\hat{\sigma}_{23}$ and the transverse normal stress $\hat{\sigma}_{33}$ when the hybrid laminate is subjected to the electric load. The normalized in-plane and the transverse shear stresses for the mechanical load $\sigma_{33}(x_1, H) = q_0 \sin \pi x_1/L$ are shown in figure 9(*b*).

For the electrical and the mechanical loads considered, the qualitative through-thickness distribution of the stress components is the same for both thick and thin laminates. The type of load strongly influences the through-thickness distribution of σ_{23} and σ_{13}. It is clear that for the electric load, the boundary conditions of null surface tractions on the top and bottom surfaces are well satisfied.

In all of the problems studied above, the piezoelectric layers extended over the entire length of the laminate. However, in practice small patches of a piezoelectric material are either affixed to the surfaces of a structure or embedded in it. Analytical solutions for cylindrical bending of laminates with segmented sensors and/or actuators have been obtained by Vel and Batra [18] by using the Eshelby–Stroh formalism. The equilibrium equations are exactly satisfied at every point in the body and the boundary conditions are satisfied in the sense of Fourier series. For the problems studied herein with simply supported and electrically insulated edges, both the equilibrium and boundary conditions are satisfied pointwise.

The authors have extended the approach presented in this paper to the analysis of three-dimensional deformations of rectangular plates with shear actuators [34].

6. Conclusions

We have obtained an exact state space solution for the three-dimensional cylindrical bending deformations of laminates with embedded piezoelectric shear actuators. The governing equations of linear piezoelectricity, the boundary conditions and interface continuity conditions between dissimilar layers are exactly satisfied.

The displacements and stresses for a homogeneous piezoelectric plate are compared with those obtained by the FSDT. The two sets of results are in good agreement only when the length-to-thickness ratio is greater than 10. The deviation between the FSDT and the exact results increases as the length-to-thickness ratio decreases.

We have also studied hybrid laminates with an axially polarized piezoelectric core sandwiched between two elastic surface layers. The application of an electric field in the thickness direction induces transverse shear deformation of the core, thus generating the desired transverse deflection. The through-thickness variation of the axial displacement takes a 'zig–zag' shape for thick and thin laminates. Thus an equivalent single-layer theory, like the FSDT, that assumes a linear variation of the axial displacement through the entire thickness of the laminate should not be used to analyse such structures, even when the thickness is small. Instead, a layerwise theory ought to be employed for sandwich laminates.

A comparison of stresses in a sandwich laminate with those in the corresponding surface-mounted extension actuator configuration reveals that the stresses within the shear actuators are significantly smaller than those in extension actuators. Thus it is advantageous to use shear actuators since large stresses can be detrimental to the brittle piezoceramic material.

The results presented herein should help validate other models for shear actuated sandwich structures.

Acknowledgments

This work was partially supported by the NSF grant CMS9713453 and the ARO grant DAAG55-98-1-0030 to Virginia Polytechnic Institute and State University.

References

[1] Crawley E F and de Luis J 1987 Use of piezoelectric actuators as elements of intelligent structures *AIAA J.* **25** 1373–85
[2] Crawley E F and Anderson E H 1990 Detailed models of piezoceramic actuation of beams *J. Intell. Mater. Syst. Struct.* **1** 4–25
[3] Lee C K 1990 Theory of laminated piezoelectric plates for the design of distributed sensors/actuators. Part 1: governing equations and reciprocal relationships *J. Acoust. Soc. Am.* **87** 1144–58
[4] Huang J H and Wu T L 1996 Analysis of hybrid multilayered piezoelectric plates *Int. J. Eng. Sci.* **34** 171–81
[5] Mitchell J A and Reddy J N 1995 A refined hybrid plate theory for composite laminates with piezoelectric laminae *Int. J. Solids Struct.* **32** 2345–67
[6] Heyliger P, Ramirez G and Saravanos D 1994 Coupled discrete-layer finite elements for laminated piezoelectric plates *Commun. Numer. Meth. Engng* **10** 971–81
[7] Robbins D H and Reddy J N 1991 Analysis of piezoelectrically actuated beams using a layer-wise displacement theory *Comput. Struct.* **41** 265–79
[8] Batra R C and Liang X Q 1997 Finite dynamic deformations of smart structures *Computat. Mech.* **20** 427–38
[9] Ray M C, Rao K M and Samanta B 1993 Exact solution for static analysis of intelligent structures under cylindrical bending *Comput. Struct.* **47** 1031–42
[10] Heyliger P and Brooks S 1996 Exact solutions for laminated piezoelectric plates in cylindrical bending *J. Appl. Mech.* **63** 903–10
[11] Heyliger P 1994 Static behavior of laminated elastic/piezoelectric plates *AIAA J.* **32** 2481–4
[12] Heyliger P 1997 Exact solutions for simply supported laminated piezoelectric plates *J. Appl. Mech.* **64** 299–306
[13] Bisegna P and Maceri F 1996 An exact three-dimensional solution for simply supported rectangular piezoelectric plates *J. Appl. Mech.* **63** 628–38
[14] Lee J S and Jiang L Z 1996 Exact electroelastic analysis of piezoelectric laminae via state space approach *Int. J. Solids Struct.* **33** 977–90
[15] Yang J S, Batra R C and Liang X Q 1994 The cylindrical bending vibration of a laminated elastic plate due to piezoelectric actuators *Smart Mater. Struct.* **3** 485–93
[16] Batra R C, Liang X Q and Yang J S 1996 The vibration of a simply supported rectangular elastic plate due to piezoelectric actuators *Int. J. Solids Struct.* **33** 1597–618
[17] Batra R C and Liang X Q 1997 The vibration of a rectangular laminated plate with embedded piezoelectric sensors and actuators *Comput. Struct.* **63** 203–16
[18] Vel S S and Batra R C 2000 Cylindrical bending of laminated plates with distributed and segmented piezoelectric actuators/sensors *AIAA J.* **38** 857–67
[19] Vel S S and Batra R C 2000 Three-dimensional analytical solution for hybrid multilayered piezoelectric plates *J. Appl. Mech.* **67** 558–67
[20] Sun C T and Zhang X D 1995 Use of thickness-shear mode in adaptive sandwich structures *Smart Mater. Struct.* **4** 202–6
[21] Zhang X D and Sun C T 1996 Formulation of an adaptive sandwich beam *Smart Mater. Struct.* **5** 814–23
[22] Zhang X D and Sun C T 1999 Analysis of a sandwich plate containing a piezoelectric core *Smart Mater. Struct.* **8** 31–40
[23] Benjeddou A, Trindade M A and Ohayon R 1997 A unified beam finite element model for extension and shear piezoelectric actuation mechanisms *J. Intell. Mater. Syst. Struct.* **8** 1012–25

[24] Aldraihem O J and Khdeir A A 2000 Smart beams with extension and thickness-shear piezoelectric actuators *Smart Mater. Struct.* **9** 1–9
[25] Benjeddou A, Trindade M A and Ohayon R 1999 A new shear actuated smart structure beam finite element *AIAA J.* **37** 378–83
[26] Trindade M A, Benjeddou A and Ohayon R 1999 Parametric analysis of the vibration control of sandwich beams through shear-based piezoelectric actuation *J. Intell. Mater. Syst. Struct.* **10** 377–85
[27] Benjeddou A, Trindade M A and Ohayon R 2000 Piezoelectric actuation mechanisms for intelligent sandwich structures *Smart Mater. Struct.* **9** 328–35
[28] Vidoli S and Batra R C 2000 Derivation of plate and rod equations for a piezoelectric body from a mixed three-dimensional variational principle *J. Elasticity* at press
[29] Vel S S and Batra R C 2001 Analysis of piezoelectric bimorphs and plates with segmented actuators *Thin-walled Struct.* **39** 23–44
[30] Ting T C T 1996 *Anisotropic Elasticity. Theory and Applications (Oxford Engineering Science Series, No 45)* (New York: Oxford University Press)
[31] Wolfram S 1999 *The Mathematica Book* 4th edn (New York: Cambridge University Press)
[32] Tiersten H F 1969 *Linear Piezoelectric Plate Vibrations* (New York: Plenum)
[33] Tang Y Y, Noor A K and Xu K 1996 Assessment of computational models for thermoelectroelastic multilayered plates *Comput. Struct.* **61** 915–33
[34] Vel S S and Batra R C 2001 Exact solution for rectangular sandwich plates with embedded piezoelectric shear actuators *AIAA J.* at press